Check for updates

View Article Online
View Journal

Journal of
Materials Chemistry C

Accepted Manuscript

This article can be cited before page numbers have been issued, to do this please use: P. M. Sonar, H. Hu, F. WONG, C. Lee, W. Chen, K. Feron, S. Manzhos, H. Wang, N. Motta, Y. Lam and H. D. Pham, *J. Mater. Chem. C*, 2018, DOI: 10.1039/C8TC01956H.

This is an Accepted Manuscript, which has been through the Royal Society of Chemistry peer review process and has been accepted for publication.

Accepted Manuscripts are published online shortly after acceptance, before technical editing, formatting and proof reading. Using this free service, authors can make their results available to the community, in citable form, before we publish the edited article. We will replace this Accepted Manuscript with the edited and formatted Advance Article as soon as it is available.

You can find more information about Accepted Manuscripts in the author guidelines.

Please note that technical editing may introduce minor changes to the text and/or graphics, which may alter content. The journal's standard Terms & Conditions and the ethical guidelines, outlined in our author and reviewer resource centre, still apply. In no event shall the Royal Society of Chemistry be held responsible for any errors or omissions in this Accepted Manuscript or any consequences arising from the use of any information it contains.

ROYAL SOCIETY OF CHEMISTRY

rsc.li/materials-c

View Article Online
DOI: 10.1039/C8TC01956H

Published on 27 July 2018. Downloaded by Kaohsiung Medical University on 7/27/2018 11:37:23 AM.

Acene-Based Organic Semiconductors for Organic Light-Emitting Diodes and Perovskite Solar Cells

Hong Duc Pham,[a♦] Hongwei Hu,[b♦] Fu-Lung Wong,[c♦] Chun-Sing Lee,[c] Wen-Cheng Chen,[c] Krishna Feron,[d,e] Sergei Manzhos,[f] Hongxia Wang,[a] Nunzio Motta,[a] Yeng Ming Lam,[b] Prashant Sonar[a*]

[a] Institute of Future Environment and School of Chemistry, Physics and Mechanical Engineering, Queensland University of Technology (QUT), 2 George Street, Brisbane, QLD-4001, Australia.

[b] School of Materials Science and Engineering, Nanyang Technological University, 50 Nanyang Avenue, 639798, Singapore.

[c] Center of Super-Diamond and Advanced Films, City University of Hong Kong, Kowloon, Hong Kong, P. R. China.

[d] CSIRO Energy Centre, NSW-2304, Australia.

[e] Centre for Organic Electronics, University of Newcastle, Callaghan, NSW 2308, Australia

[f] Department of Mechanical Engineering, Faculty of Engineering, National University of Singapore, Block EA #07-08, 9 Engineering Drive 1, Singapore 117576.

♦All three authors contributed equally *Email sonar.prashant@qut.edu.au, sonarpm74@gmail.com

Keywords: anthracene, naphtho[1,2-*b*:5,6-*b′*]dithiophene, green/blue emission, organic light-emitting diodes, dopant-free, perovskite solar cells

Journal of Materials Chemistry C Accepted Manuscript

View Article Online
DOI: 10.1039/C8TC01956H

Published on 27 July 2018. Downloaded by Kaohsiung Medical University on 7/27/2018 11:37:23 AM.

Journal of Materials Chemistry C Accepted Manuscript

ABSTRACT

In this work, three novel acene-based organic semiconductors, including 2,7-bis(trimethylstannyl)naphtho[2,1-*b*:6,5-*b*']dithiophene (**TPA-NADT-TPA**), 4,4'-(anthracene-2,6-diyl)bis(*N*,*N*-bis(4-methoxyphenyl)aniline (**TPA-ANR-TPA**) and N^2,N^2,N^6,N^6-tetrakis(4-methoxyphenyl)anthracene-2,6-diamine (**DPA-ANR-DPA**), are designed and synthesized for use in organic light-emitting diodes (OLEDs) and perovskite solar cells (PSCs). In OLEDs, the devices based on **TPA-NADT-TPA**, **TPA-ANR-TPA** and **DPA-ANR-DPA** showed pure blue, blue green, and green emission, respectively. Also, the maximum brightness of the devices with a turn-on voltage at 3.8 V reached 8682 cd/m^2 for **TPA-NADT-TPA**, 11180 cd/m^2 for **TPA-ANR-TPA**, and 18600 cd/m^2 for **DPA-ANR-DPA** respectively. These new materials are also employed as hole transporting materials (HTMs) in inverted PSCs, where they were used without additives. The inverted devices based on these HTMs achieved an overall efficiency of 10.27 % for **TPA-NADT-TPA**, 7.54 % for **TPA-ANR-TPA**, and 6.05 % for **DPA-ANR-DPA** under identical condition (AM 1.5G and 100 mW cm^{-2}). While the PSCs with **TPA-NADT-TPA** as HTM achieved the highest efficiency, the **DPA-ANR-DPA** based OLED devices showed the brightest emission and efficiency. Based on the obtained promising performance, it is clear that this molecular design presents a new research strategy to develop materials that can be used in multiple types of devices.

INTRODUCTION

Up to date, a considerable inventory of organic semiconductors, including small molecules and polymers have been synthesized and implemented in various organic electronic devices such as organic solar cells (OSCs or OPV), dye-sensitized solar cells (DSSCs), perovskite solar cells (PSCs), organic field-effect transistors (OFETs), organic light-emitting diodes (OLEDs) and so on. These materials can be categorized into two groups based on their applications. One includes a single organic semiconducting material that can be designed for a single specific application. There is rich literature in which such materials and devices have been reported. The other group can be defined as multipurpose materials where a single molecule can be used in several types of devices. It has been widely reported that materials developed for OFET devices can also be used successfully for OPV and exhibit very high performance in both types of devices.[1-3] Currently, there are few studies relative to organic semiconducting materials which can be used for dual application such as OSCs and PSCs.[4-7]

View Article Online
DOI: 10.1039/C8TC01956H

Published on 27 July 2018. Downloaded by Kaohsiung Medical University on 7/27/2018 11:37:23 AM.

Journal of Materials Chemistry C Accepted Manuscript

However, there are hardly any studies on organic semiconductors which can be used for a dual application in OLEDs and PSCs. Herein, we are reporting the use of a single type of materials for two different types of devices, namely, OLED and PSC.

The application of OLED in TVs, smartphones, digital cameras, and so on[8-11] has been very successful commercially because this technology guarantees high-energy efficiency and pure bright colours; it allows large area processing and is suitable for flexible displays.[12-14] As a consequence, highly efficient clear red, blue, and green coloured OLED devices have been developed. However, there is still great demand to reduce the cost and further improve performance of such devices for the production of state of the art large area processable light emitting materials. This task requires molecular engineering to develop novel organic semiconductors.[15-18] High performance red/orange emissive materials already exist in the market, but for pure blue/green emission, low cost materials still remain a critical challenge, particularly in terms of high efficiency, easy availability, and colour purity.[11, 19, 20]

One of the promising optoelectronic applications of organic semiconductors is to design low cost high performance charge transporting materials for PSCs. Perovskite based solar harvesting technology has gained significant attention and became one of the hot topics in both academic and industrial research. The fast growth of PSC technology is due to astonish improvements in power conversion efficiency (PCE) within the last few years (from 3.8 % to 22.7 % in seven years).[21] Basically, the device configuration of PSCs is categorized into conventional (n-i-p) and inverted (p-i-n) types. Compared to the conventional one, the inverted architectures provide many significant benefits. First, the inverted devices are fabricated by using low-temperature solution-processing techniques and thus can be simply employed on flexible substrates, leading to very promising large-area production of these devices.[22-25] Second, they can avoid high-temperature instability and large hysteresis issues, which impede practical application of PSCs.[25-27] Up to date, several research groups have developed numerous organic semiconductors that serve as hole transporting layer (HTL) of inverted PSC layouts. This layer is critical to achieve very high open circuit voltage (V_{oc}) and PCE in the inverted PSCs.[28, 29] Furthermore, in addition to hole transport ability after exciton dissociation, the HTL plays a key role to protect the active perovskite layer from moisture/oxygen ingress and electrode penetration.[30, 31] Currently, the champion efficiencies of inverted PSCs exhibited roughly 19.4% and 18.1% by using poly[bis(4-phenyl)(2,4,6-trimethylphenyl)amine] (PTAA)[32] and poly(3,4-ethylenedioxythiophene : polystyrene sulfonate) (PEDOT : PSS)[33] as the hole transporting materials (HTMs), respectively.

View Article Online
DOI: 10.1039/C8TC01956H

Published on 27 July 2018. Downloaded by Kaohsiung Medical University on 7/27/2018 11:37:23 AM.

Journal of Materials Chemistry C Accepted Manuscript

Unfortunately, the PTAA polymer is extremely costly, being about 50 times the price of gold whereas PEDOT:PSS is hydrophilic and of a strong acidic nature which reduces the device's long-term stability.[24, 34, 35] In addition to the above limitations, molecular weight of polymers varies batch-to-batch, which may further affect the performance of the device. Compared to polymeric semiconductors based HTMs, small molecules, which present several intrinsic advantages such as good yield,[5] defined molecular structure,[36] tunable energetics[37] and good batch-to-batch reproducibility,[5, 36] can alleviate these limitations. One of the most well-known small molecular HTMs is 2,2',7,7'-tetrakis(*N*,*N*'-di-pmethoxyphenylamino)-9,9'-spirbiuorene (Spiro-OMeTAD). Although Spiro-OMeTAD based devices achieved a remarkable performance of 20.8%,[38] there are significant drawbacks of Spiro-OMeTAD including high cost, multistep synthesis and cell stability.[39] Spiro-OMeTAD usually requires salt type additives to enhance the conductivity in order to achieve high performance of the device. Due to the use of salts as additives, the PSC devices are vulnerable to the environmental stability, and performance degrades rapidly.[31, 40] These bottlenecks can be addressed by developing new generation HTMs via molecular design.

In the present work, we are reporting three novel small molecules, namely 2,7-bis(trimethylstannyl)naphtho[2,1-*b*:6,5-*b*']dithiophene (**TPA-NADT-TPA**), 4,4'-(anthracene-2,6-diyl)bis(*N*,*N*-bis(4-methoxyphenyl)aniline **(TPA-ANR-TPA**) and N^2,N^2,N^6,N^6-tetrakis(4-methoxyphenyl)anthracene-2,6-diamine (**DPA-ANR-DPA**) using fused anthracene and naphthodithiophene cores, respectively. The optical, thermal, and electronic properties are characterised experimentally as well as using density functional theory (DFT) calculations. The materials exhibit high thermal stability, good solubility, and high fluorescent efficiency. These materials were used as an active light emitting material in OLED devices and demonstrated promising performance with bright blue-green emission and high brightness. The same materials were also used as hole transporting layers in PSC devices, where they could achieve the highest PCE exceeding 10 % . To the best of our knowledge, these newly developed organic small molecules are reported here for the first time with dual functions as dopants in OLED and pristine hole transporting materials (HTMs) in PSCs.

View Article Online
DOI: 10.1039/C8TC01956H

Published on 27 July 2018. Downloaded by Kaohsiung Medical University on 7/27/2018 11:37:23 AM.

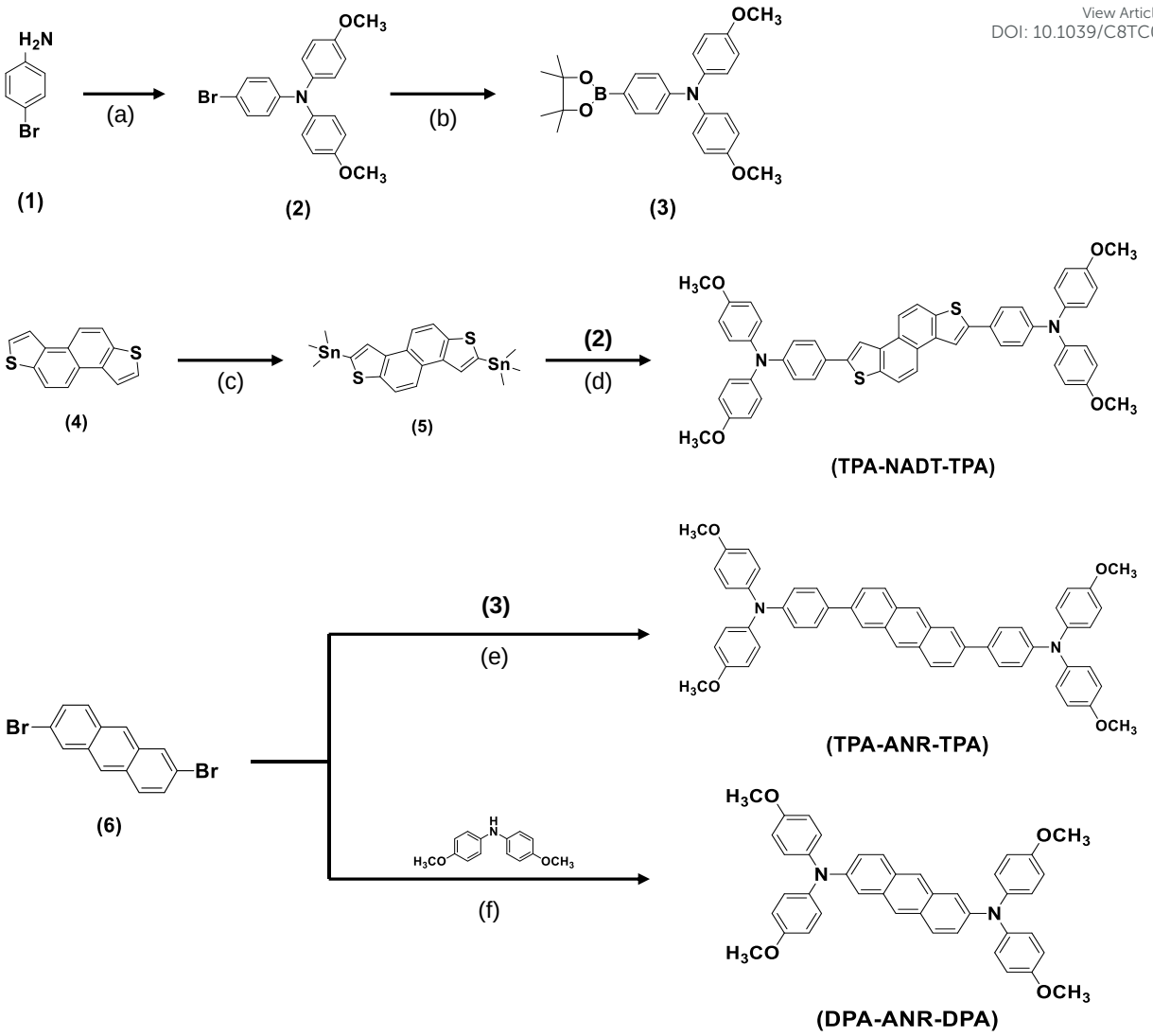

Scheme 1. Synthesis routes of **TPA-NADT-TPA**, **TPA-ANR-TPA** and **DPA-ANR-DPA**. Reagent and conditions: (a) 1-iodo-4-methoxybenzene, KOH, CuCl, 1,10-phenanthroline monohydrate, toluene, 120 ^{o}C, overnight; (b) bis(pinacolato)diboron, KOAc, Pd(dppf)Cl_2, DMF, 80 ^{o}C, 12 h; (c) n-BuLi, THF, Me_3SnCl, -78 ^{o}C, 12 h; (d) 2,7-bis(trimethylstannyl)naphtho[2,1-*b*:6,5-*b*']dithiophene, DMF, Pd(PPh_3)$_4$, 110 ^{o}C, 48 h; (e) 2M K_2CO_3, toluene, Pd(PPh_3)$_4$, 120 ^{o}C, 48 h; (f) Diphenylamine, $^{t}Bu_3P$, NaO^{t}Bu, $Pd_2(dba)_3$, Toluene, 110 ^{o}C, 48 h.

Journal of Materials Chemistry C Accepted Manuscript

View Article Online
DOI: 10.1039/C8TC01956H

Published on 27 July 2018. Downloaded by Kaohsiung Medical University on 7/27/2018 11:37:23 AM.

Journal of Materials Chemistry C Accepted Manuscript

RESULTS AND DISCUSSIONS

Molecular Design and Synthesis.

Acene cores have been used successfully for synthesizing various classes of organic semiconductors for a wide range of applications including OFETs[41-43], OLEDs[44-46], PSCs,[47, 48] and OPV[49-52]. Due to their fused aromatic structure and planar nature, acenes can be considered as a potent class of conjugated building blocks for constructing new high performance organic semiconductors. In this work, we have used two simply fused cores based on fused phenylene aromatic, "anthracene", and naphthalene fused with thiophene, "naphtho[1,2-*b*:5,6-*b′*]dithiophene", respectively. The rationale for the choice of anthracene (ANR) and naphtho[1,2-*b*:5,6-*b′*]dithiophene (NADT) cores is due to their planar nature. Planar groups are extremely beneficial for organic electronics because they can provide high charge-carrier mobility and ultimately high performance.[53-56] Additionally, their fused nature is significant for better π-π stacking due to large orbital overlap. Herein, ANR group has been rationally selected due to its key important features such as strong emission and high charge carrier mobility.[46] Besides the ANR core, we have also used NADT fused core due to its more extended conjugation than ANR. Fusion of two thiophene rings with naphthalene makes it more electron rich and highly planar. NADT would be an ideal core to compare with ANR core because both of these units possess high charge carrier mobility and high performance in devices.[57, 58] Furthermore, the attachment of thiophene moieties in NADT structure has been shown to improve OLEDs[59, 60], OSCs,[56, 61] and PSCs[25, 62] performance. ANR and NADT groups were selected as cores whereas triphenylamine (TPA) and diphenylamine (DPA) moieties are selected as end-capping groups in order to study their effect on the device performance. The TPA unit has been widely used in OSCs, DSSCs and PSCs[36, 63] owing to its 3D propeller design, strong electron-donating and transporting capabilities and amorphous structure forming ability.[64, 65] Its derivatives are also implemented widely as hole-transporting or light-emitting materials in OLEDs.[64-72] However, the long intermolecular distance of the non-planar TPA may lead to low hole mobility. Thus, DPA groups are introduced at the end of ANR and NADT cores for comparison with TPA. Although the DPA group is a weaker electron donor compared to TPA, DPA derivatives have demonstrated high efficiencies in OSCs, DSSCs and PSCs.[36] However, there are very few studies reporting DPA based derivatives for OLEDs.

View Article Online
DOI: 10.1039/C8TC01956H

Published on 27 July 2018. Downloaded by Kaohsiung Medical University on 7/27/2018 11:37:23 AM.

Journal of Materials Chemistry C Accepted Manuscript

The synthesis routes of **TPA-NADT-TPA**, **TPA-ANR-TPA** and **DPA-ANR-DPA** are depicted in Scheme 1. First, the synthesis of the precursor 4-bromo-*N*,*N*-bis(4-methoxyphenyl)aniline (2) and 4-methoxy-*N*-(4-methoxyphenyl)-*N*-(4-(4,4,5,5-tetramethyl-1,3,2-dioxaborolan-2-yl)phenyl)aniline (3) followed earlier attempts.[25, 39] The NADT core (2,7-bis(trimethylstannyl)naphtho[2,1-*b*:6,5-*b*I]dithiophene, (5)) was prepared by using naphtho[2,1-*b*:6,5-*b'*]dithiophene (4) with trimethyltin chloride (Me_3SnCl) and n-butyllithium (n-BuLi) in tetrahydrofuran (THF) solvent at room temperature for 12 h. The target **TPA-NADT-TPA** was synthesized by Stille coupling reaction between compound (2) and (5) tetrakistriphenylphosphine palladium [$Pd(PPh_3)_4$] catalyst at 110 ^oC for 48 h in dimethylformamide (DMF) solvent. Meanwhile, the synthesis of **TPA-ANR-TPA** was based on Suzuki coupling reaction between compound (3) and (6) using tetrakis triphenylphosphine palladium [$Pd(PPh_3)_4$] catalyst and 2 M K_2CO_3 base at 120 ^oC for 48 h in toluene solvent. The target compound **DPA-ANR-DPA** was prepared via Buchwald-Hartwig coupling reaction between compound (6) and bis(4-methoxyphenyl)amine using tris(dibenzylideneacetone)dipalladium [$Pd_2(dba)_3$] catalyst, tri-tert-butylphosphine ($^tBu_3P$), and sodium tert-butoxide (NaO^tBu) at 110 ^oC for 48 h in toluene solvent. After purification, **TPA-NADT-TPA**, **TPA-ANR-TPA** and **DPA-ANR-DPA**'s yield was 38.2 %, 38.3 % and 50.2 %, respectively. Their purity was proved by proton and C13 nuclear magnetic resonance (NMR) spectroscopy (Figure S1-S3, ESI†). The molecular weight was confirmed by mass spectroscopy. While the solubility of **DPA-ANR-DPA** was extremely good in most common organic solvents such as chloroform, dichloromethane, and chlorobenzene, **TPA-NADT-TPA** and **TPA-ANR-TPA** exhibited lower solubility due to their highly conjugated backbone and rigid chemical structure.

Ab initio Calculations

View Article Online
DOI: 10.1039/C8TC01956H

Published on 27 July 2018. Downloaded by Kaohsiung Medical University on 7/27/2018 11:37:23 AM.

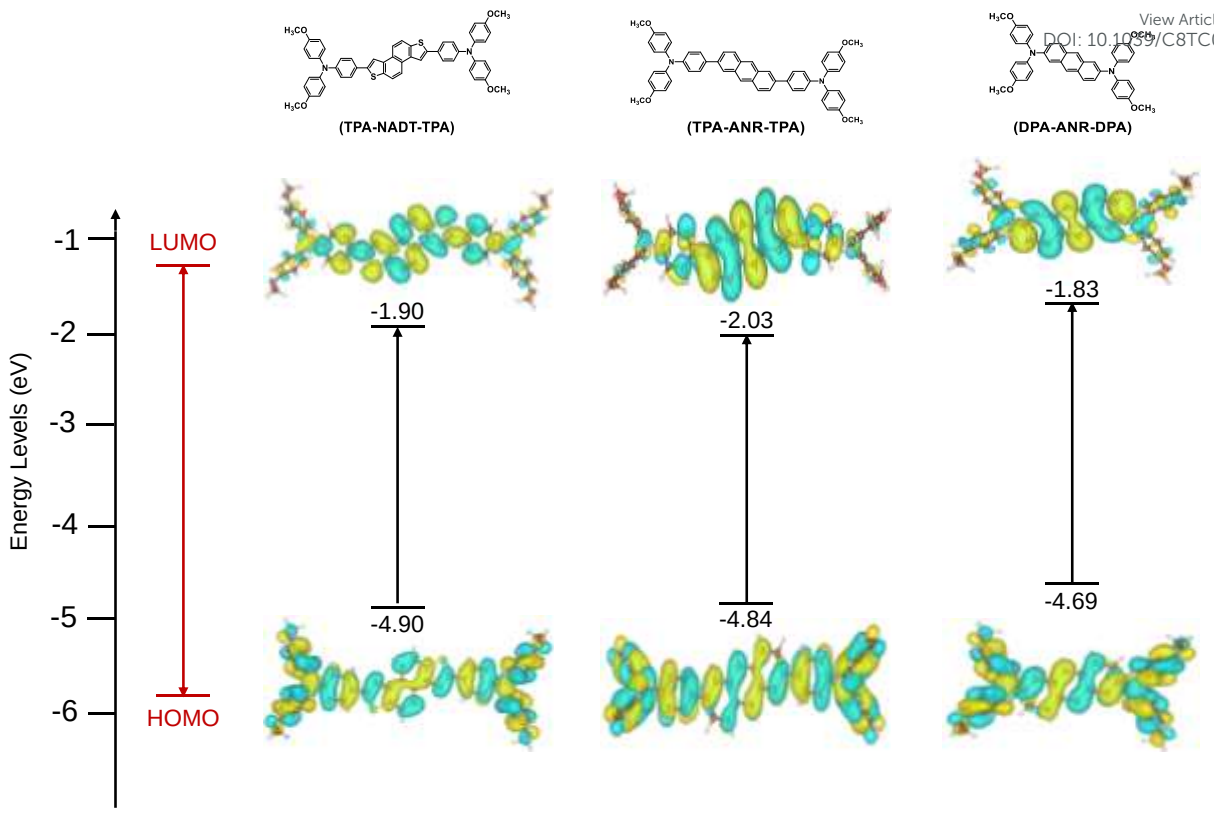

Fig. 1. Calculated energy levels of HOMO and LUMO orbital isosurfaces of **TPA-NADT-TPA**, **TPA-ANR-TPA**, and **DPA-ANR-DPA**.

Fig. 1 shows the molecular structures and frontier orbital electron density distributions of the three new small molecules computed with DFT at the B3LYP/LANL2DZ level with a PCM model of the chloroform solvent.[73-75] The computed frontier orbital energies, optical absorption and photoluminescence data are summarized in Table S1 (ESI†). In all three molecules, both LUMO and HOMO orbitals are delocalized over the entire aromatic system, which is extremely important for efficient charge transport.[76] Indeed, the electron distribution of the LUMO is primarily localized on NADT and ANR cores whereas the HOMO is fully delocalized over the entire molecules including the end-capping groups, reflecting the electron-rich nature of TPA and DPA. The calculated HOMO values of **TPA-NADT-TPA**, **TPA-ANR-TPA**, and **DPA-ANR-DPA** are -4.90, -4.84 and -4.69 eV, respectively; the LUMO values are -1.90, -2.03 and -1.83 eV, respectively. The theoretical HOMO-LUMO trend helps understand the effect of end capping groups and the nature of core on the energy level tuning. Specifically one observes a lower LUMO with TPA vs DPA, which corresponds to delocalization of the LUMO onto core-adjacent phenyls of the TPA. The DPA unit leads to a higher HOMO, likely due to steric hindrance with the core of DPA's both phenyl units vs a

Journal of Materials Chemistry C Accepted Manuscript

View Article Online
DOI: 10.1039/C8TC01956H

Published on 27 July 2018. Downloaded by Kaohsiung Medical University on 7/27/2018 11:37:23 AM.

Journal of Materials Chemistry C Accepted Manuscript

single core-adjacent unit with TPA. This trend is similar to the experimental results below, while the absolute values of HOMO and LUMO differ due to difference in aggregate state and approximations, as expected. We also note that the computed LUMO is higher than the estimate below based on the optical gap as the latter is downshifted due to broadening effects (being determined from the *onset* of absorption).

Electrochemical Properties.

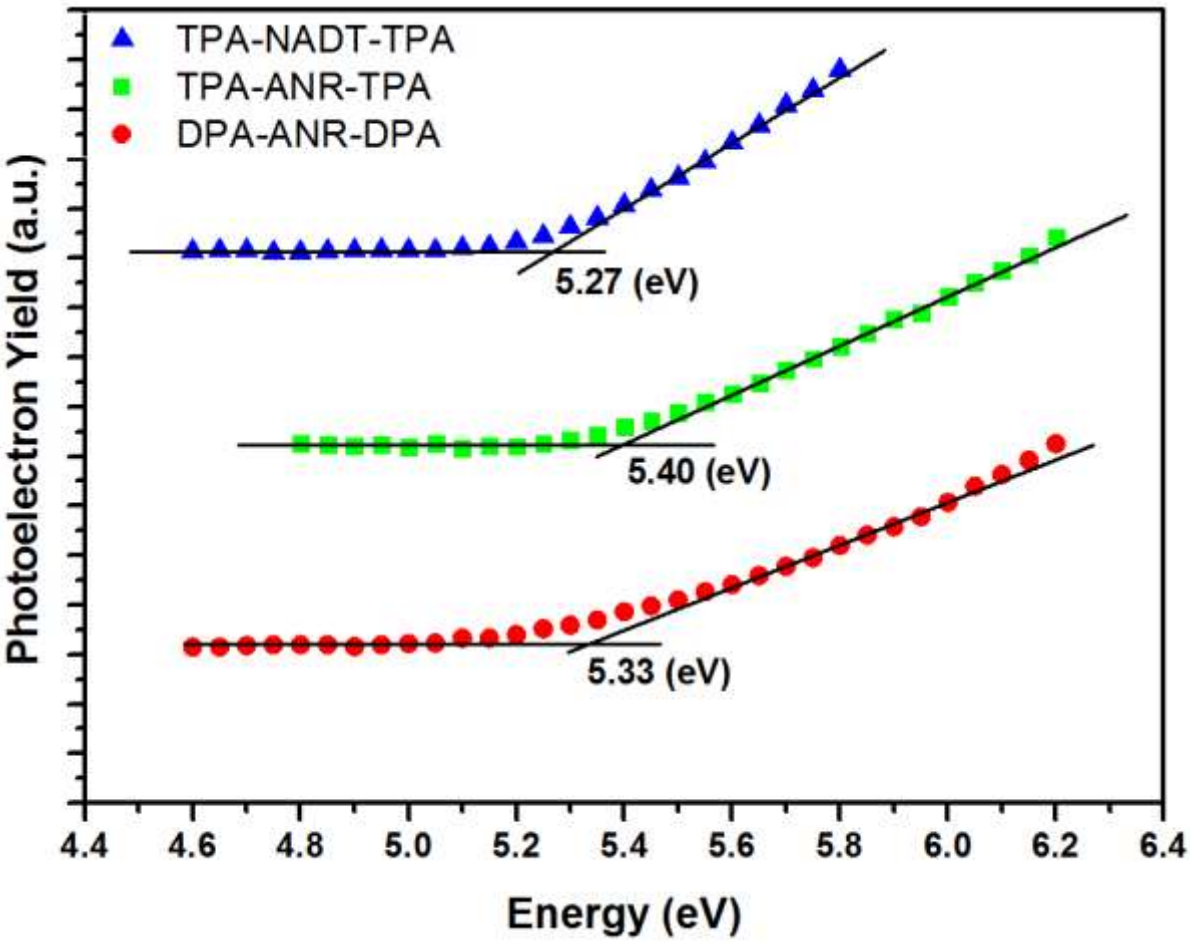

Fig. 2. Photoelectron spectroscopy in air (PESA) spectra of three new semiconductors.

We measured the HOMO energy levels in thin film using photoelectron spectroscopy in air (PESA), whereas, the LUMO values were calculated from the difference between the HOMO values and the optical bandgap. The corresponding data are summarized in Table 1. According to PESA, the HOMO values of **TPA-NADT-TPA**, **TPA-ANR-TPA** and **DPA-ANR-DPA** are estimated to be at -5.27, -5.40 and -5.33 eV, respectively. These HOMO

View Article Online
DOI: 10.1039/C8TC01956H

values are well matched with that of perovskite ($CH_3NH_3PbI_3$, -5.44 eV) and host (MADN, -5.6 eV) materials, suggesting a good hole injection ability of these new materials. Regarding the ANR core, the replacement of end-capping TPA by DPA has affected the HOMO energy level, which proves that TPA units are stronger electron donating ability than DPA ones. This is consistent with the observed red shifts in UV-Vis spectra of both compounds and the trend observed for the energy levels of other HTMs based on ANR core in an earlier report.[47] From the obtained LUMO values of these compounds, it is clear that they have appropriate value, which is sufficient to block the electron injection due to high-energy offset.

Optical Properties.

Published on 27 July 2018. Downloaded by Kaohsiung Medical University on 7/27/2018 11:37:23 AM.

Journal of Materials Chemistry C Accepted Manuscript

View Article Online
DOI: 10.1039/C8TC01956H

Published on 27 July 2018. Downloaded by Kaohsiung Medical University on 7/27/2018 11:37:23 AM.

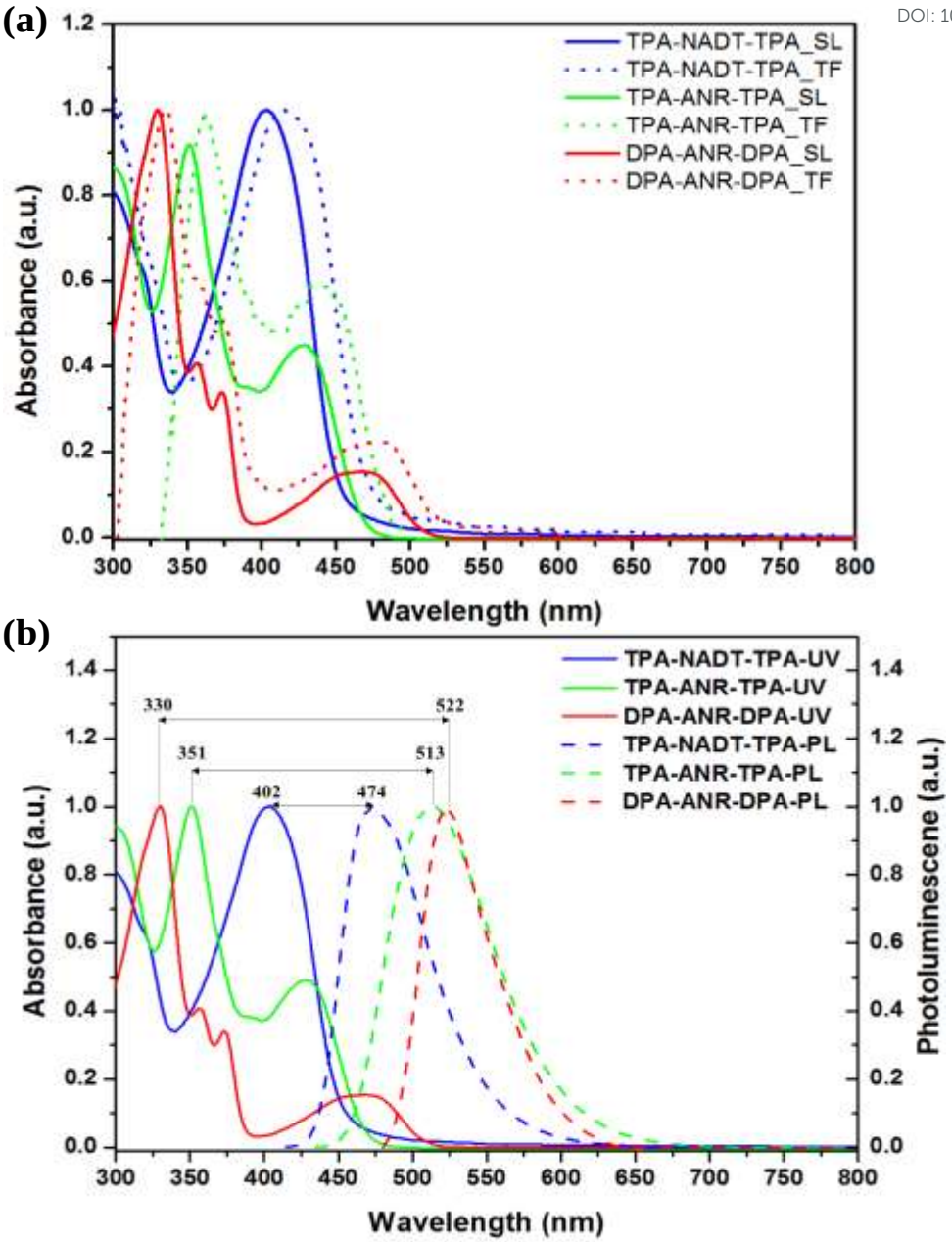

Fig. 3. (a) UV-Vis absorption spectra in CF solutions (SL, solid line) and films (TF, dash line) and (b) Normalised absorption (solid line) and emission spectra (dash line) in CF solutions of **TPA-NADT-TPA**, **TPA-ANR-TPA** and **DPA-ANR-DPA**.

The optical properties of all newly developed materials characterized by UV-Vis and photoluminescence spectroscopy respectively. The normalized UV-vis absorption spectra of **TPA-NADT-TPA**, **TPA-ANR-TPA** and **DPA-ANR-DPA** in chloroform (CF) solutions and solid films are shown in Fig. 3a and the photophysical data are recorded in Table 1. Overall, there is a similar pattern of the spectra between the thin films and solutions, suggesting that

Journal of Materials Chemistry C Accepted Manuscript

View Article Online
DOI: 10.1039/C8TC01956H

Published on 27 July 2018. Downloaded by Kaohsiung Medical University on 7/27/2018 11:37:23 AM.

Journal of Materials Chemistry C Accepted Manuscript

there is no significant crystallization in thin films.[77] On account of intermolecular interactions in the solid state, the slightly bathochromic shift is observed in the absorption spectra of solid-state films compared to that of solutions. Additionally, the red shift is attributed to the increased π-electron density (π–π* transitions) of the compound. There is the obvious red-shifted absorption among these compounds in order: **DPA-ANR-DPA** < **TPA-ANR-TPA** < **TPA-NADT-TPA** which could be ascribed to: (a) the DPA unit having the lower electron-donating ability compared to the TPA unit due to number of phenyl groups presents in the structure; (b) the NADT moiety retaining the higher electron-donating ability in comparison to the ANR moiety due to electron rich two thiophene units fused with naphthalene. The optical absorption of these materials exhibit peaks in the ultraviolet (300 – 350 nm) and visible (400 – 500 nm) regions. **TPA-NADT-TPA** displays a strong peak (402 nm) in the visible area and a lower one in the UV region whereas ANR derivatives behave conversely. Compound **DPA-ANR-DPA** unveils absorption maxima at 330 nm for solution and 335 nm for thin film whereas the absorption peaks in solution and thin film of **TPA-ANR-TPA** are 351 and 361 nm, respectively. Indeed, the optical band gaps of **TPA-NADT-TPA**, **TPA-ANR-TPA** and **DPA-ANR-DPA** are 2.63, 2.58 and 2.37 eV, respectively, which is determined from the absorption onset wavelength (E_g^{opt}=1240/ λ_{onset}) of the corresponding absorption spectrum.

The normalized photoluminescence (PL) spectra for these three small molecules were conducted in CF solution and illustrated in Fig. 3b. The emission maximum peaks are found to be 474 nm for **TPA-NADT-TPA**, 513 nm for **TPA-ANR-TPA**, and 522 nm for **DPA-ANR-DPA**. Stokes shift, which is defined as the gap between the ground state S_0 and the first excited state S_1, is calculated from the difference between the maximum of absorption and emission spectra. These compounds possess large Stoke shifts in order: **TPA-NADT-TPA** (72 nm) < **TPA-ANR-TPA** (162 nm) < **DPA-ANR-DPA** (192 nm), indicating that these materials can play dual functionality in both organic light emitting diodes and perovskite solar cells. Note that the measured trend in the PL peaks corresponds to that computed with TD-DFT (Table S1). According to TD-DFT, the peaks are due to LUMO→HOMO transitions; the corresponding HOMO→LUMO transitions in the absorption spectrum correspond in the experimental spectrum to less intense peaks around 475 nm for **DPA-ANR-DPA** and around 440 nm for **TPA-ANR-TPA** and to the main peak around 425 nm for **TPA-NADT-TPA**.

View Article Online
DOI: 10.1039/C8TC01956H

Published on 27 July 2018. Downloaded by Kaohsiung Medical University on 7/27/2018 11:37:23 AM.

Journal of Materials Chemistry C Accepted Manuscript

Thermal Properties.

In addition to the optical properties, the thermal properties of these new small molecules were also studied by thermogravimetric analysis (TGA) (Fig. S5, ESI†) and differential scanning calorimetry (DSC) (Fig. S6, ESI†). Thermal properties of the molecules are vital in order to study the effect of thermal annealing of the thin film on the performance of devices. The summarized thermal data are listed in Table 1. According to TGA, these molecules start to decompose at a temperature above 431 ^{o}C for **TPA-NADT-TPA,** 438 ^{o}C for **TPA-ANR-TPA** and 370 ^{o}C for **DPA-ANR-DPA**, showing their high thermal stability. The high and almost identical thermal stability of both **TPA-NADT-TPA** and **TPA-ANR-TPA** is attributed to their rigid molecular pi-conjugated backbone. In addition to this observation, the DSC results also exhibited a low glass transition temperature (T_g) of 101, 108 and 122 ^{o}C for **DPA-ANR-DPA**, **TPA-ANR-TPA**, and **TPA-NADT-TPA**, respectively. Notably, while **TPA-ANR-TPA** and **TPA-NADT-TPA** do not show a crystallization temperature (T_c), that of **DPA-ANR-DPA** is observed at 183 ^{o}C. The high melting point and glass transition temperature of all three compounds suggest good heat tolerance for device fabrication and operation if annealing of thin film is required.

Table 1. Thermal, optical and electrochemical properties of new organic materials.

HTMs	λ_{max} [nm]		λ_{PL} c)	Stoke shift	E_g^{opt} d)	E_{HOMO} e)	E_{LUMO} f)	T_d	T_g	T_m	T_c
	Solution a)	Film b)	[nm]	[nm]	[eV]	[eV]	[eV]	[°C]	[°C]	[°C]	[°C]
TPA-NADT-TPA	402	416	474	72	2.63	-5.27	-2.64	431	122	237	-
TPA-ANR-TPA	351	361	513	162	2.58	-5.40	-2.82	438	108	217	-
DPA-ANR-DPA	330	335	522	192	2.37	-5.33	-2.96	370	101	248	183

[a)]Absorption spectrum was measured in chloroform (CF) solution; [b] Film was prepared by spin-coating CF solution containing the sample onto glass substrate at a spin speed of 1000 rpm at room temperature; [c]Emission spectrum was analysed in CF solution; [d]Optical bandgap was calculated from the formula of $1240/\lambda_{onset}$; [e]The oxidation potential was also measured by photoelectron spectroscopy in air (PESA); [f] $E_{LUMO}^{PESA}=E_{HOMO}^{PESA}+E_g^{opt}$.

View Article Online
DOI: 10.1039/C8TC01956H

Published on 27 July 2018. Downloaded by Kaohsiung Medical University on 7/27/2018 11:37:23 AM.

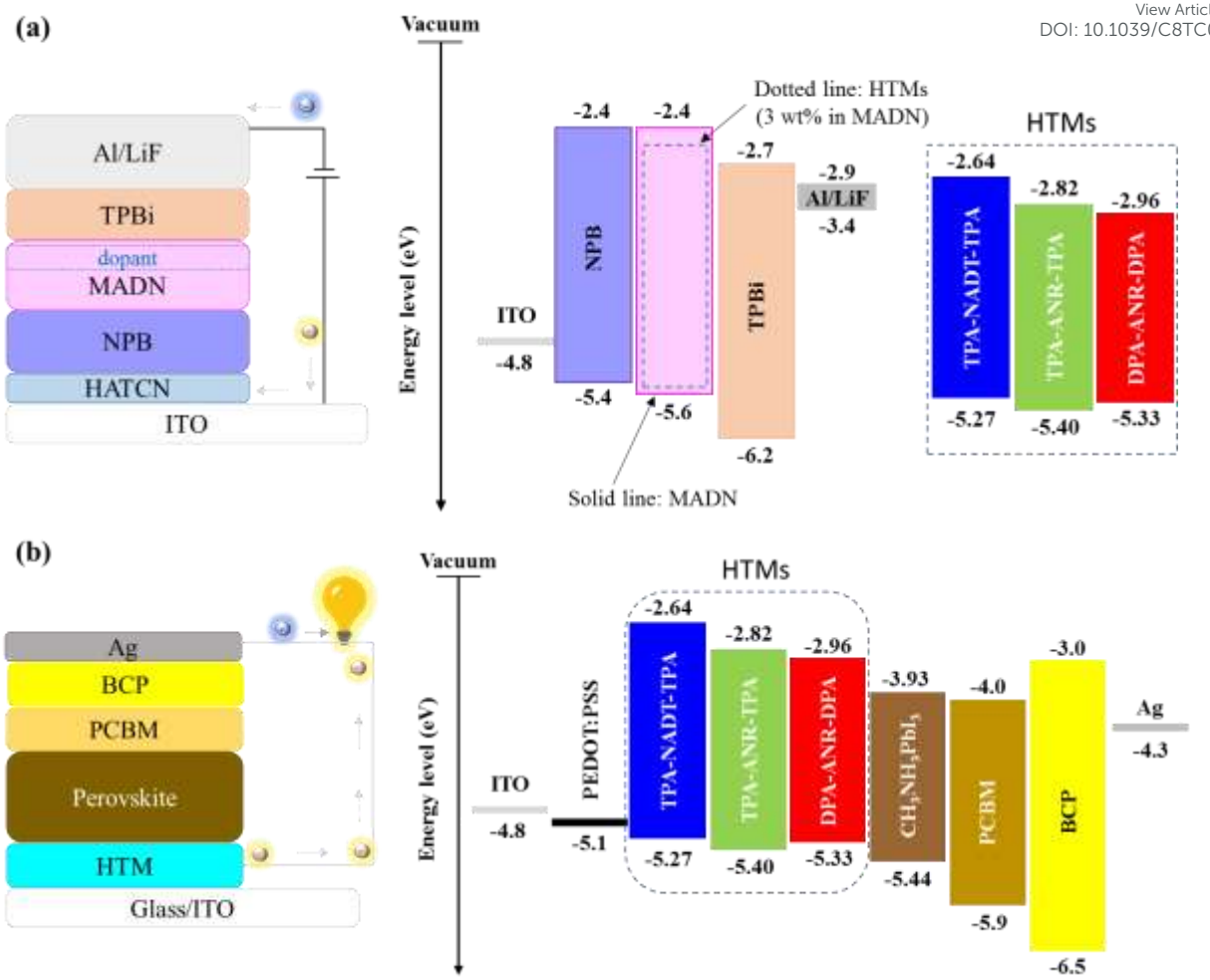

Fig. 4. Diagram of the device structure and energy levels in (a) OLED and (b) PSC devices.

OLEDs Performance.

Owing to intense luminescence under UV-lamp (both solution and solid state) of **TPA-NADT-TPA**, **TPA-ANR-TPA**, and **DPA-ANR-DPA**, we decided to investigate them further in OLED devices using the thin film as an active light-emitting layer. To prove this, the photoluminescence quantum yield (PLQY) of these compounds was estimated in chloroform solution and neat thin film. The corresponding data are shown in Table 2. The same molecules are also studied in PSC devices, which are shown in the next part, in order to investigate the effect of three different chemical structures on the device performance.

For OLED devices, a host-guest layer was introduced because this system has the benefit of improving electroluminescence and operational stability.[59] 3 wt% of each **TPA-NADT-TPA**, **TPA-ANR-TPA**, and **DPA-ANR-DPA** materials were doped into a wide-band-gap host material as an emissive layer in OLED devices, which is illustrated in Fig. 4a.

Journal of Materials Chemistry C Accepted Manuscript

View Article Online
DOI: 10.1039/C8TC01956H

Published on 27 July 2018. Downloaded by Kaohsiung Medical University on 7/27/2018 11:37:23 AM.

Journal of Materials Chemistry C Accepted Manuscript

Their use as dopant in a wide band gap host improves hole injection ability and reduces the concentration-quenching effect on emitters. A simple OLED device architecture was fabricated as follows: ITO/HATCN/NPB/MADN: dopant/TPBi/LiF/Al. According to this configuration, 1,4,5,8,9,11-hexaazatriphenylene hexacarbonitrile (HATCN) and 4,4′-bis[*N*-(1-naphthyl)-*N*-phenylamino]biphenyl (NPB) acts as a hole injecting and transporting layers whereas 2-methyl-9,10-bis(naphthalen-2-yl)anthracene (MADN) was used as the host compound with our newly synthesized dopant as a light-emitting layer. Additionally, 1,3,5-tris(*N*-phenyl benzimidizol-2-yl)benzene (TPBi) was used as the hole-blocking or electron-transporting layer whereas LiF was used as electron injecting layer. The chemical structure of all these functional materials was illustrated in Fig. S7 (ESI†).

The characterization of a series of OLED devices is revealed in Fig. 5 and 6. The relevant data is summarized in Table 2. As shown in Fig. 5, the emission color varies from sky blue (**TPA-NADT-TPA**), blue-green (**TPA-ANR-TPA**) to pure green (**DPA-ANR-DPA**). The obtained brightness is indeed very high and promising. The electroluminescence (EL) peaks for **TPA-NADT-TPA**, **TPA-ANR-TPA** and **DPA-ANR-DPA** based OLED devices are recorded at 465 nm, 486 nm, and 522 nm with the Commission Internationale de l'Éclairage (CIE) ordinating (0.16, 0.23), (0.17, 0.39), and (0.32, 0.62), respectively. Furthermore, Fig. 6 exhibits the maximum brightness of the devices was 8682 cd/m^2 for **TPA-NADT-TPA**, 11180 cd/m^2 for **TPA-ANR-TPA**, and 18600 cd/m^2 for **DPA-ANR-DPA** respectively. In addition, the power efficiency (PE) for **TPA-NADT-TPA**, **TPA-ANR-TPA**, **DPA-ANR-DPA** based OELD devices is 3.1, 5.9, and 8.0 lumen per watt (lm/W) at 4V, respectively. All the OLED devices exhibit a low turn on voltage close to 3.8 V. The lower voltage is due to an appropriate HOMO energy level. The current efficiency (CE) of **TPA-NADT-TPA**, **TPA-ANR-TPA**, **DPA-ANR-DPA** based OELD devices is 4.0, 7.8, and 11.5 candela per ampere (cd/A) respectively. Among them, **DPA-ANR-DPA** based devices exhibited higher CE, PE and brightness. Meanwhile, the emission of **TPA-ANR-TPA** results in the blue-green light and its OLEDs shows lowest efficiency, which is due to its more molecular aggregation.[78] For ANR derivatives, while DPA groups is not as strong electron-donating ability as TPA ones, the CE, PE and maximum brightness of **DPA-ANR-DPA** in OLEDs is higher than those of **TPA-ANR-TPA**. On the other hand, the other ANR-based compound, namely DPA, exhibited pure blue emission in the previous report with brightness up to 6627 cd/m^2.[46] In the present study, by replacing two phenyl rings with DPA and TPA units, the brightness increases to 11180 cd/m^2 for **DPA-ANR-DPA** and 18600 cd/m^2 for

View Article Online
DOI: 10.1039/C8TC01956H

Published on 27 July 2018. Downloaded by Kaohsiung Medical University on 7/27/2018 11:37:23 AM.

TPA-ANR-TPA. Also, the emission color diverges from pure blue into pure green (**DPA-ANR-DPA**) and blue-green (**TPA-ANR-TPA**), which indicates that the introduction of stronger electron donating units has effects on the emission color of ANR derivatives based OLEDs. The promising performance of all of the newly designed materials in OLED devices clearly indicates the great potential of acene based organic semiconductors.

Table 2. Performance of OLED device.

Device	Turn on voltage (V) @1 cd/m^2	CE (Cd/A)	PE (lm/W)	CIE (x,y)	EL peak (nm)/ FWHM (nm)	Max. brightness (cd/m^2)	PLQY (%)	
							Solution	Film
TPA-NADT-TPA	3.8	4 (@6 V)	3.1 (@4 V)	0.16, 0.23	465/65	8682	10.89	58.49
TPA-ANR-TPA	3.8	7.8 (@6 V)	5.9 (@4 V)	0.17, 0.39	486/63	11180	16.20	66.98
DPA-ANR-DPA	3.8	11.5 (@4.5 V)	8 (@4.5 V)	0.32, 0.62	522/61	18600	18.60	6.51

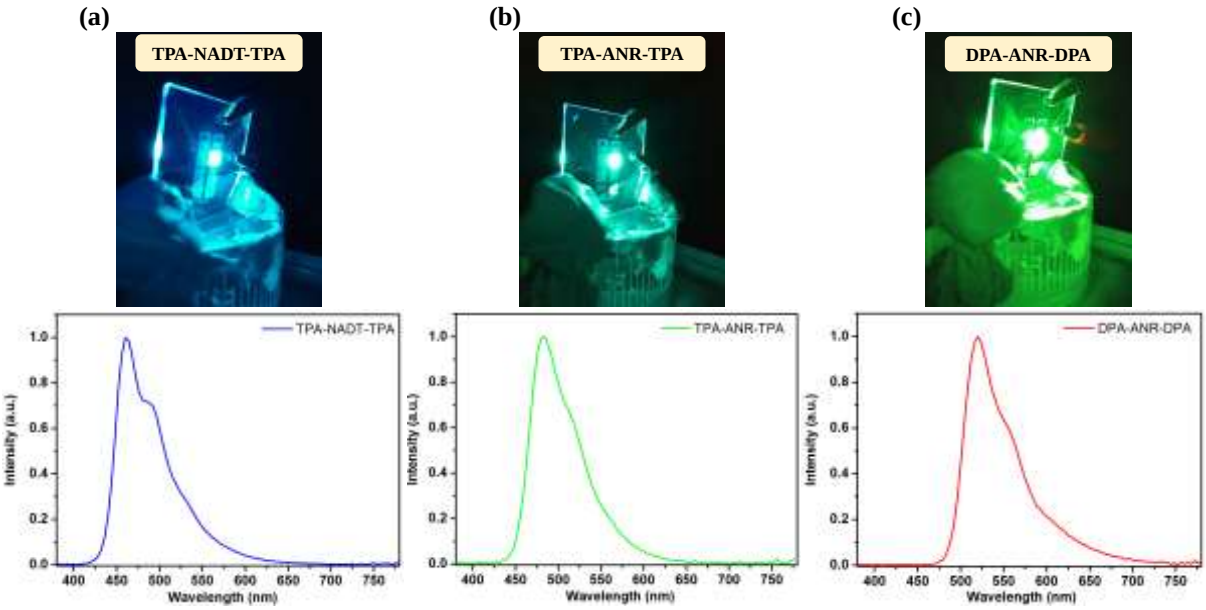

Fig. 5. Electroluminescent spectrum of OLED with (a) **TPA-NADT-TPA**, (b) **TPA-ANR-TPA** and (c) **DPA-ANR-DPA** dopants in MADN.

Journal of Materials Chemistry C Accepted Manuscript

View Article Online
DOI: 10.1039/C8TC01956H

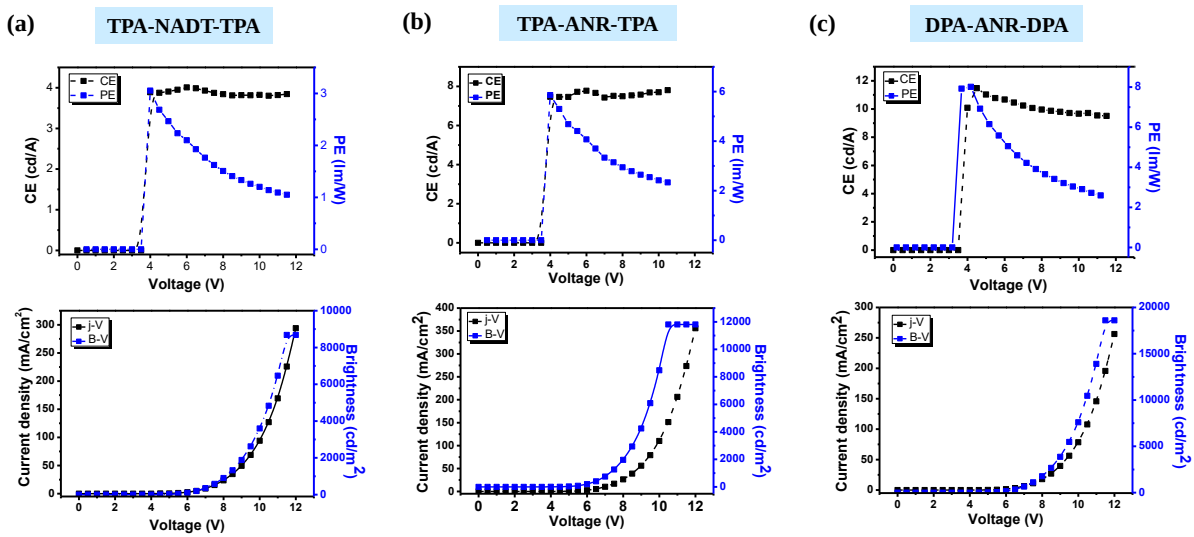

Fig. 6. Current efficiency (CE) and current density characteristics of (a) **TPA-NADT-TPA**, (b) **TPA-ANR-TPA** and (c) **DPA-ANR-DPA** dopants in MADN based OLED devices.

PSCs Performance.

Since the molecular design of **TPA-NADT-TPA**, **TPA-ANR-TPA**, and **DPA-ANR-DPA** contains TPA and DPA end-capping groups at the end of the acene cores which facilitate hole conduction, all these materials could be potential materials for HTL in perovskite solar cells as suggested by earlier reports.[25, 36, 53, 62, 79-81] Therefore, these compounds were implemented in the inverted device layouts: glass/ITO/HTL/perovskite/PCPM/BCP/Ag as in our previous study.[25] In this structure, the active layer is $CH_3NH_3PbI_3$ whereas 2,9-dimethyl-4,7-diphenyl-1,10-phenanthroline (BCP) acts as an electron extracting and hole blocking layer and the fullerene derivative [6,6]-phenyl C61 butyric acid methyl ester (PCBM) as an electron transporting compact layer. The device construction and energy levels of each layer are illustrated in Fig. 4b. Moreover, the chemical structure of PCPM and BCP was depicted in Fig. S8 (ESI†).

The performance of inverted devices based on different HTMs was investigated and shown in Fig. 7. According to the cross-sectional scanning electron microscopy (SEM) image of a complete device shown in Fig. 7a, above the indium tin-oxide (ITO) coated glass there is a thin layer of HTM and the perovskite layer, electron transporting layer (including PCBM and BCP) and back silver electrode. Fig. 7b presents the current density–voltage (*J*–*V*)

Published on 27 July 2018. Downloaded by Kaohsiung Medical University on 7/27/2018 11:37:23 AM.

Journal of Materials Chemistry C Accepted Manuscript

View Article Online
DOI: 10.1039/C8TC01956H

Published on 27 July 2018. Downloaded by Kaohsiung Medical University on 7/27/2018 11:37:23 AM.

Journal of Materials Chemistry C Accepted Manuscript

characteristic measured under simulated sun illumination (AM 1.5 G, 100 mWcm^{-2}). The corresponding parameters are listed in Table 3. Overall, the devices based on these new HTMs are found to achieve the PCE of 10.27 % for **TPA-NADT-TPA**, 7.54 % for **TPA-ANR-TPA** and 6.05 % for **DPA-ANR-DPA**, compared to that of standard PEDOT:PSS based device (11.29%). The lower efficiency of **TPA-ANR-TPA** and **DPA-ANR-DPA** based devices compared to standard PEDOT:PSS ones may be caused by the aggregation of these chemical structures.[82] This is related to their low solubility in chlorobenzene/dichlorobenzene, which makes it more challenging to obtain smooth and uniform films. In addition, the devices based on **TPA-NADT-TPA** and PEDOT:PSS HTMs result in a better PCE in comparison with the others because of the presence of thiophene units.[25, 62] For ANR derivatives, even though **DPA-ANR-DPA** shows a better solubility than **TPA-ANR-TPA**, the device efficiency of **TPA-ANR-TPA** HTL is higher than that with **DPA-ANR-DPA**. This may be attributed to the less strong electron-donating ability of DPA units, leading to a lower hole mobility of the DPA compound.[47] This result also coincides well with earlier studies reporting that the efficiency achieved using HTMs based on TPA end-capping groups is greater than that with DPA under similar conditions in inverted[83] and mesoporous[47, 84-87] configurations.

According to Table 3, the devices with **TPA-NADT-TPA** HTL present a better open-circuit voltage (V_{oc}) than that with PEDOT:PSS, demonstrating a better band alignment of **TPA-NADT-TPA** HTL with the perovskite layer. Although the HOMO values of **TPA-ANR-TPA** and **DPA-ANR-DPA** are close to that of perovskite materials, their V_{oc} values are not better than that of **TPA-NADT-TPA**. This may be triggered by the poor uniformity of these materials[88] and high interfacial recombination in the devices,[89, 90] leading to the low efficiency of ANR derivatives. Additionally, the short-circuit current (J_{sc}) for **TPA-NADT-TPA**, **TPA-ANR-TPA** and **DPA-ANR-DPA** are 20.04, 16.68, and 17.49 mA cm^{-2}, respectively. These values also match well with the values obtained from the integrated external quantum efficiency (EQE) spectra (as shown in Fig. 7c). While the J_{sc} of **TPA-NADT-TPA** HTL based devices is better than that of standard PEDOT:PSS HTL, the devices with **TPA-NADT-TPA** HTL exhibit a lower PCE than those using PEDOT:PSS HTL. The reason is due to the significant drop in fill factor (*FF*) of **TPA-NADT-TPA**, which may be caused by a less smooth film and lower mobility of this new material.[88, 91] The series resistance (R_s) for the four HTL-based devices was derived from the *J-V* curves according to the previous report.[92] The PEDOT:PSS based PSC shows a low R_s value of 5.36 Ω·cm^2, while

View Article Online
DOI: 10.1039/C8TC01956H

Published on 27 July 2018. Downloaded by Kaohsiung Medical University on 7/27/2018 11:37:23 AM.

the **TPA-NADT-TPA**, **TPA-ANR-TPA** and **DPA-ANR-DPA** based PSCs show higher R_s of 10.68 Ω·cm^2, 8.52 Ω·cm^2 and 9.43 Ω·cm^2. The higher R_s for the three new HTL resulted in lower *FF* and subsequently limited the PCE.[92]

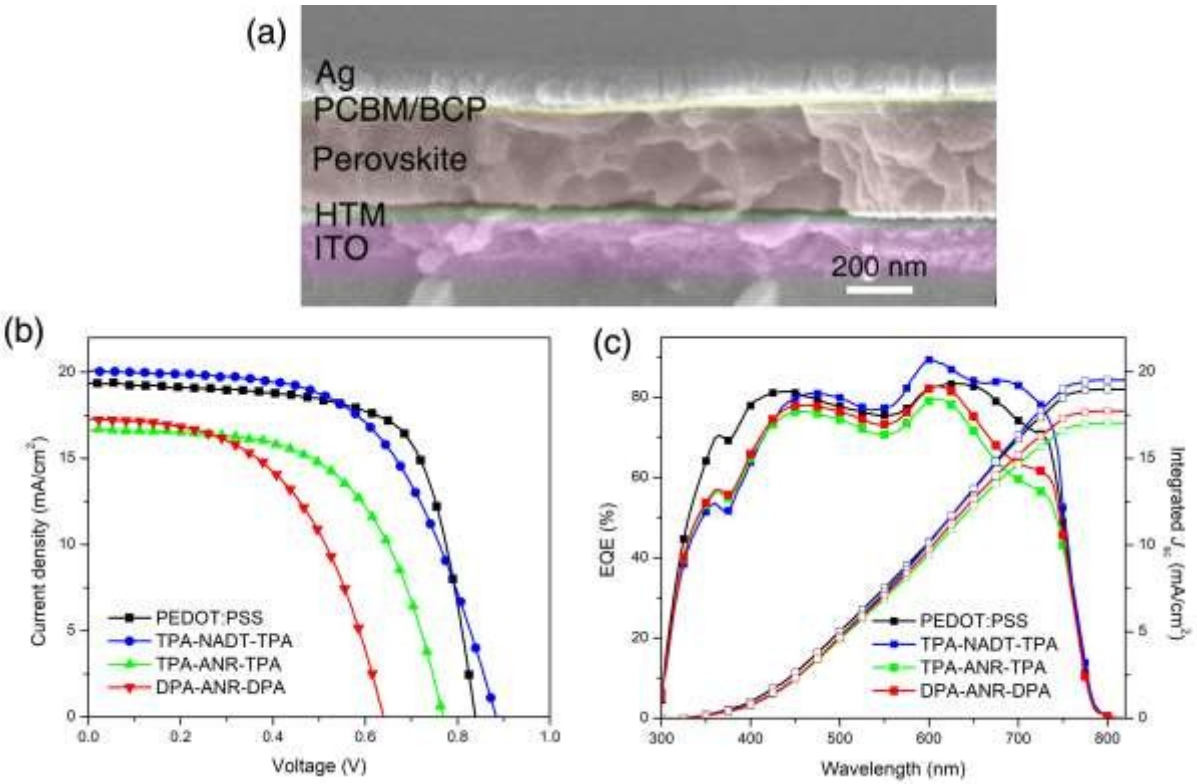

Fig. 7. a) Cross-sectional scanning electron microscopy image of the device, b) Current density–voltage curves (*J*–*V*) of PSCs with different HTMs, and c) their external quantum efficiency (EQE) spectra (lines with open symbols indicate the integrated J_{sc} from EQE and solar spectrum).

Table 3. J–V parameters of PSCs with different HTLs as **TPA-NADT-TPA**, **TPA-ANR-TPA** and **DPA-ANR-DPA** and PEDOT:PSS.[a)]

HTLs	V_{OC} [V]	J_{SC} [mA/cm^2]	*FF*	PCE[b)] [%]
PEDOT:PSS	0.83	19.38	0.70	11.29
TPA-NADT-TPA	0.88	20.04	0.58	10.27
TPA-ANR-TPA	0.77	16.68	0.589	7.54
DPA-ANR-DPA	0.63	17.49	0.549	6.05

Journal of Materials Chemistry C Accepted Manuscript

View Article Online
DOI: 10.1039/C8TC01956H

[a)]Cell size (active area): 7 mm^2. Photovoltaic performance at 1000 wm^{-2} (AM1.5G) and constant scan speed of 30 mV/s mesoscopic $CH_3NH_3PbI_3$ devices; [b)]An average device efficiency of total 10 devices.

CONCLUSIONS

In summary, we have designed and developed a novel series of acene based solution processable organic semiconductors with triphenylamine and diphenylamine end capping groups. The compounds namely 2,7-bis(trimethylstannyl)naphtho[2,1-*b*:6,5-*b*']dithiophene (**TPA-NADT-TPA**), 4,4'-(anthracene-2,6-diyl)bis(*N*,*N*-bis(4-methoxyphenyl)aniline (**TPA-ANR-TPA**), and N^2,N^2,N^6,N^6-tetrakis(4-methoxyphenyl)anthracene-2,6-diamine (**DPA-ANR-DPA**) were synthesized by Stille, Suzuki, and Buchwald organometallic coupling. The effect of central acene cores varying from lower conjugation anthracene to highly extended conjugated napthodithiophene attached to end capping triphenyl and diphenyl amine moiety on the opto-electronic properties were studied. The optical band gap is in the range of 2.3 to 2.7 eV, placing these newly compounds in the area of wide band gap compounds. Interestingly, these materials, which possess suitable LUMO-HOMO energy levels, can play dual functionality in OLEDs and PSCs. For OLED devices based on these materials, their electroluminescence maximum varies in the range of 465 nm to 522 nm with sky-blue, blue-green to pure green thin film colour emission. Additionally, they exhibit a low turn-on voltage at 3.8 V and strong emission with the maximum brightness of 8682 cd/m^2 for **TPA-NADT-TPA**, 11180 cd/m^2 for **TPA-ANR-TPA**, and 18600 cd/m^2 for **DPA-ANR-DPA**. These small molecules have been also fabricated successfully in perovskite solar cell devices as HTMs without additives. The inverted devices based on these HTMs achieve an overall efficiency of 10.27 % for **TPA-NADT-TPA**, 7.54 % for **TPA-ANR-TPA** and 6.05 % for **DPA-ANR-DPA**. The excellent performance of these newly designed materials, in both OLED and PSC devices, confirms that our innovative molecular design of organic semiconductors is a promising and versatile approach. These materials play a dual role and this opens up a new research strategy where single materials can be used for multiple devices.

EXPERIMENTAL SECTION

1. Synthesis

Published on 27 July 2018. Downloaded by Kaohsiung Medical University on 7/27/2018 11:37:23 AM.

Journal of Materials Chemistry C Accepted Manuscript

View Article Online
DOI: 10.1039/C8TC01956H

Published on 27 July 2018. Downloaded by Kaohsiung Medical University on 7/27/2018 11:37:23 AM.

Journal of Materials Chemistry C Accepted Manuscript

The synthesis of compound (2) and (3) was followed an earlier published synthetic procedure.[25, 39]

Synthesis of 2,7-Bis(trimethylstannyl)naphtho[1,2-b:5,6-b']dithiophene (5): n-Butyllithium (2.4 M solution in hexane, 3.03 mL, 7.28 mmol) was added dropwise to a solution of compound (4) (500 mg, 2.08 mmol) in dry THF (50 mL) at -78 °C. The mixture was stirred at this temperature for 30 min and then at room temperature for 1 h. After cooling down to -78 °C, Me_3SnCl (1 M solution in hexane, 8.32 mL, 8.32 mmol) was added dropwise. After stirring for 30 min at this temperature, the reaction was allowed to warm up to room temperature and stirred overnight. The reaction mixture was then extracted with chloroform and water. The organic layer was dried over anhydrous Na_2SO_4 and concentrated by evaporation. After removing the solvent under reduced pressure, the residue was purified by recrystallization from acetone (800 mg, 69 %).^{1}H NMR (600 MHz, $CDCl_3$): 7.98-7.96 (d, 2H), 7.84-7.83 (d, 2H), 7.48 (s, 2H), 0.39 (s, 18H).

Synthesis of 2,7-bis(trimethylstannyl)naphtho[2,1-*b*:6,5-*b*']dithiophene (**TPA-NADT-TPA**): Compound (5) (350 mg, 0.616 mmol) and compound (2) (640 mg, 0.166 mmol) were vacuumed for 20 minutes prior to adding anhydrous DMF (35 ml). The solution was degassed with argon for 20 minutes and then tetrakis (triphenylphosphine) palladium (25 mg, 0.022 mmol) was added. The reaction was refluxed at 110 °C for 48 hours then extracted by chloroform. The extract was dried and concentrated. The purification of the residue on silica using hexane : dichloromethane (2:1 v/v) as the eluent. It was recrystallized by hot methanol to yield the desired compound as a yellow solid (200 mg, 38.4 %). ^{1}H NMR (600 MHz, $CDCl_3$): δ 7.89-7.88 (d, J = 8.4 Hz, 2H), 7.75-7.74 (d, J = 8.4 Hz, 2H), 7.50-7.43 (m, 6H), 7.02 (s, *8*H), 6.88 (s, 4H), 6.79-6.78 (d, J = 9.0 Hz, 8H), 3.74 (s, 12H). ^{13}C NMR (120 MHz, $CDCl_3$): δ 156.26, 149.30, 143.51, 140.27, 138.28, 137.38, 130.53, 126.97, 125.62, 122.35, 121.21, 120.35, 119.07, 118.18, 114.73, 55.52. ESI-MS: $C_{54}H_{42}N_2O_4S_2^{+\bullet}$ *m/z* 846.33 (calculated *m/z* 846.26).

Synthesis of 4,4'-(anthracene-2,6-diyl)bis(*N*,*N*-bis(4-methoxyphenyl)aniline (**TPA-ANR-TPA**): In a round bottom flask, compound (5) (200 mg, 0.599 mmol), compound (4) (723 mg, 1.677 mmol), and 2 M aqueous K_2CO_3 solution (12 mL) were dissolved in anhydrous toluene (20 mL). The solution was degassed by argon for 20 minutes, then tetrakis(triphenylphosphine)palladium (21 mg, 0.018 mmol) was added. Subsequently, the mixture was degassed for 30 min before the reaction was stirred at 120 °C for 2 days. After

View Article Online
DOI: 10.1039/C8TC01956H

Published on 27 July 2018. Downloaded by Kaohsiung Medical University on 7/27/2018 11:37:23 AM.

the reaction mixture was cooled to room temperature and extracted with chloroform and water. The organic layer was dried over anhydrous Na_2SO_4. After removing the solvent under reduced pressure, the residue was purified using silica gel column chromatography with a mixture of hexane, chloroform, and ethyl acetate as eluent. Then the crude product was recrystallized from hot methanol to yield the desired compound as a yellow solid (180 mg, 38.3%). ^{1}H NMR (600 MHz, $CDCl_3$): δ 8.33 (s, 2H), 8.05 (s, 2H), 7.96-7.94 (d, *J* = 9 Hz, 2H), 7.66-7.64 (dd, *J* = 1.8, 10.2 Hz, 2H), 7.53-7.52 (d, *J* = 8.4 Hz, 4H), 7.05-7.04 (d, *J* = 9 Hz, 8H), 6.98-6.97 (d, *J* = 8.4 Hz, 4H), 6.80-6.78 (m, 8H), 3.74 (s, 12H). ^{13}C NMR (120 MHz, $CDCl_3$): δ 155.96, 140.84, 137.18, 132.73, 131.97, 131.05, 128.53, 127.68, 126.69, 125.93, 125.37, 124.35, 120.78, 114.74, 55.52. ESI-MS: $C_{54}H_{44}N_2O_4^{+\bullet}$ *m/z* 784.50 (calculated *m/z* 784.33).

Synthesis of 4,4'-(anthracene-2,6-diyl)bis(*N*,*N*-bis(4-methoxyphenyl)aniline (**DPA-ANR-DPA**): Compound (6) (200 mg, 0.599 mmol), bis(4-methoxyphenyl)amine (343 mg,1.497 mmol), and NaO^{t}Bu (149 mg, 1.797 mmol) were added and vacuumed for 30 min. Afterwards, anhydrous toluene (25 ml) and ^{t}Bu$_3$P (1M toluene solution, 20μl, 0.02 mmol) were added to dissolve the solid and degassed by argon for 30 min. Then, $Pd_2(dba)_3$ (22.2 mg, 0.024 mmol) was added and the mixture was vacuumed and degassed for 30 min. Subsequently, the reaction was stirred at 110 °C for 2 days. After the reaction mixture was cooled to room temperature and extracted with chloroform and water. The organic layer was dried over anhydrous Na_2SO_4 and the solvent removed under reduced pressure. The residue was purified using silica gel column chromatography with a mixture of hexane and chloroform as eluent. Then the crude product was recrystallized from hot methanol to yield the desired compound as a yellow solid (190 mg, 50.2 %).^{1}H NMR (600 MHz, $CDCl_3$): δ 7.94 (s, 2H), 7.69-7.68 (d, *J* = 9, 2H), 7.25 (s, 2H), 7.19-7.18 (dd, *J* = 1.8, 9 Hz, 2H), 7.13-7.12 (d, *J* = 9 Hz, 8H), 6.88-6.87 (d, *J* = 9 Hz, 8H), 6.80-6.78 (m, 8H), 3.84 (s, 12H). ^{13}C NMR (120 MHz, $CDCl_3$): δ 155.81, 144.92, 141.11, 131.55, 128.98, 128.30, 126.84, 126.41, 123.69, 115.27, 114.67, 55.52. ESI-MS: $C_{42}H_{36}N_2O_4^{+\bullet}$ *m/z* 632.42 (calculated *m/z* 632.27).

2. **OLED Device Fabrication**

OLED devices based on **TPA-NADT-TPA**, **TPA-ANR-TPA** and **DPA-ANR-DPA** were fabricated by thermal evaporation**.** The three synthesized materials were used as dopants with device configuration of: ITO/HATCN (10 nm)/NPB (45 nm)/MADN: 3 wt% dopant (35

Journal of Materials Chemistry C Accepted Manuscript

View Article Online
DOI: 10.1039/C8TC01956H

Published on 27 July 2018. Downloaded by Kaohsiung Medical University on 7/27/2018 11:37:23 AM.

Journal of Materials Chemistry C Accepted Manuscript

nm)/TPBi (35 nm)/LiF (1 nm)/Al (150 nm). In this configuration, 1,4,5,8,9,11-hexaazatriphenylene hexacarbonitrile (HATCN) and 4,4′-bis[*N*-(1-naphthyl)-*N*-phenylamino]biphenyl (NPB) act as a hole injecting and transporting layers, respectively. Additionally, while 2-methyl-9,10-bis(naphthalen-2-yl)anthracene (MADN) was used as the host compound, 1,3,5-tris(*N*-phenyl benzimidizol-2-yl)benzene (TPBi) was used as the electron-transporting layer. Furthermore, LiF and Al were used as the electron injecting layer and cathode, respectively. All organic and inorganic layers were deposited onto the UV ozone treated ITO glass substrates in a multiple thermal source vacuum deposition chamber under $2x10^{-6}$ Torr. The device electroluminescent performances such as current-voltage, brightness, electroluminescent spectra, C.I.E co-ordinates were measured and recorded by a computer-controlled DC power supply with a Spectra PR650 CCD camera.

3. **Perovskite Device Fabrication**

Poly(3,4-ethylenedioxythiophene) polystyrene sulfonate (PEDOT:PSS, AI 4083) and bathocuproine (BCP) were purchased from Heraeous and Lumtec, respectively. PbI_2 was purchased from TCI (Tokyo Chemical Industry). Other chemicals were purchased from Sigma-Aldrich. PCBM (60) was purchased from Nano-C. Methylammonium iodide (MAI) was synthesized according to a previously reported method. The perovskite precursor solution ($MAPbI_3$) was prepared by dissolving MAI and PbI_2 with stoichiometric ratio in gammabutyrolactone/dimethyl sulfoxide (7:3 v/v, 1.1 M) at 80°C.

Perovskite solar cells were prepared on a pre-cleaned patterned ITO substrate. A filtered PEDOT:PSS solution was spin-coated on ITO at 3000 rpm and annealed at 150°C for 10 min. For new HTMs (**TPA-NADT-TPA**, **TPA-ANR-TPA**, and **DPA-ANR-DPA**) based devices, while **TPA-ANR-TPA** was prepared with a mixed solvent of chloroform and 1,2-dichlorobenzene at 2 mg/ml (1:1 v/v), **TPA-NADT-TPA** and **DPA-ANR-DPA** were dissolved in 1,2-dichlorobenzene at 5 mg/ml. Afterwards, they were spin-coated on the ITO substrate. The film thickness was varied by changing the spin speed from 2000 rpm to 5000 rpm. The perovskite precursor solution (pre-heated at 80°C) was spin-coated onto these hole-transporting layers at 1000 rpm for 10 s and 4000 rpm for 30 s, 250 μL toluene was dripped on the sample surface at 15 s of the second step spin-coating. Subsequently, the perovskite layer was annealed at 80°C for 5 min, 100°C for 30 min. The PCBM solution was coated from a chlorobenzene solution (20 mg/mL) at 1000 rpm for 60 s. The devices were completed

View Article Online
DOI: 10.1039/C8TC01956H

by evaporating BCP (6 nm) and Ag (120 nm) sequentially under high vacuum (1×10^{-6} mbar). The active area was 7 mm^2 as defined by the overlapping between the back electrode and ITO. Current density-voltage (*J-V*) characteristics were measured using a calibrated solar simulator (AAA, SAN-EI ELECTRIC CO.,LTD.) coupled with Keithley 2400 Source meter. External quantum efficiency (EQE) was obtained by combining a monochromatic light source, a light chopper and a lock-in amplifier (SR830-DSP).

AUTHOR INFORMATION

Corresponding Author

*E-mail: sonar.prashant@qut.edu.au.

Author Contributions

The manuscript was written through contributions of all authors. All authors have given approval to the final version of the manuscript.

ACKNOWLEDGMENT

H.D.M is thankful to QUT for QUTPRA scholarship for conducting his doctoral research. We are very thankful to Central Analytical Research Facility (CARF), Institute of Future Environments (IFE) and Queensland University of Technology (QUT) for providing facility and equipment support. P.S. is thankful to QUT for the financial support from the Australian Research Council (ARC) for the Future Fellowship (FT130101337) and QUT core funding (QUT/ 322120-0301/07). The Ministry of Education of Singapore supports S. M.

References

Published on 27 July 2018. Downloaded by Kaohsiung Medical University on 7/27/2018 11:37:23 AM.

Journal of Materials Chemistry C Accepted Manuscript

View Article Online
DOI: 10.1039/C8TC01956H

Published on 27 July 2018. Downloaded by Kaohsiung Medical University on 7/27/2018 11:37:23 AM.

Journal of Materials Chemistry C Accepted Manuscript

1. M. Horie, J. Kettle, C.-Y. Yu, L. A. Majewski, S.-W. Chang, J. Kirkpatrick, S. M. Tuladhar, J. Nelson, B. R. Saunders and M. L. Turner, *J. Mater. Chem.*, 2012, **22**, 381-389.

2. G. Conboy, R. G. D. Taylor, N. J. Findlay, A. L. Kanibolotsky, A. R. Inigo, S. S. Ghosh, B. Ebenhoch, L. Krishnan Jagadamma, G. K. V. V. Thalluri, M. T. Sajjad, I. D. W. Samuel and P. J. Skabara, *J. Mater. Chem. C*, 2017, **5**, 11927-11936.

3. P. Han, X. Gong, B. Lin, Z. Jia, S. Ye, Y. Sun and H. Yang, *RSC Adv.*, 2015, **5**, 50098-50104.

4. B. Xu, E. Sheibani, P. Liu, J. Zhang, H. Tian, N. Vlachopoulos, G. Boschloo, L. Kloo, A. Hagfeldt and L. Sun, *Adv. Mater.*, 2014, **26**, 6629-6634.

5. S. S. Reddy, K. Gunasekar, J. H. Heo, S. H. Im, C. S. Kim, D. H. Kim, J. H. Moon, J. Y. Lee, M. Song and S. H. Jin, *Adv. Mater.*, 2016, **28**, 686-693.

6. M. Cheng, C. Chen, X. Yang, J. Huang, F. Zhang, B. Xu and L. Sun, *Chem. Mater.*, 2015, **27**, 1808-1814.

7. H. Azimi, T. Ameri, H. Zhang, Y. Hou, C. O. R. Quiroz, J. Min, M. Hu, Z.-G. Zhang, T. Przybilla, G. J. Matt, E. Spiecker, Y. Li and C. J. Brabec, *Adv. Energy Mater.*, 2015, **5**.

8. T. Miwa, S. Kubo, K. Shizu, T. Komino, C. Adachi and H. Kaji, *Sci. Rep.*, 2017, **7**, 284.

9. W. Song and J. Y. Lee, *Adv. Optical Mater.*, 2017, **5**.

10. J. K. Salunke, F. L. Wong, K. Feron, S. Manzhos, M. F. Lo, D. Shinde, A. Patil, C. S. Lee, V. A. L. Roy, P. Sonar and P. P. Wadgaonkar, *J. Mater. Chem. C*, 2016, **4**, 1009-1018.

11. Z. Ma, P. Sonar and Z.-K. Chen, *Curr. Org. Chem.*, 2010, **14**, 2034-2069.

12. N. Li, S. Oida, G. S. Tulevski, S. J. Han, J. B. Hannon, D. K. Sadana and T. C. Chen, *Nat. Commun.*, 2013, **4**, 2294.

13. S. Kappaun, C. Slugovc and E. J. List, *Int. J. Mol. Sci.*, 2008, **9**, 1527-1547.

14. M. P. d. Cunha, T. T. Do, S. D. Yambem, H. D. Pham, S. Chang, S. Manzhos, R. Katoh and P. Sonar, *Mater. Chem. Phys.*, 2018, **206**, 56-63.

15. P. Tao, Y. Zhang, J. Wang, L. Wei, H. Li, X. Li, Q. Zhao, X. Zhang, S. Liu, H. Wang and W. Huang, *J. Mater. Chem. C*, 2017, **5**, 9306-9314.

16. J. Han, S. Guo, J. Wang, L. Wei, Y. Zhuang, S. Liu, Q. Zhao, X. Zhang and W. Huang, *Adv. Optical Mater.*, 2017, **5**.

17. P. Tao, W.-L. Li, J. Zhang, S. Guo, Q. Zhao, H. Wang, B. Wei, S.-J. Liu, X.-H. Zhou, Q. Yu, B.-S. Xu and W. Huang, *Adv. Funct. Mater.*, 2016, **26**, 881-894.

18. Y. Li, J.-Y. Liu, Y.-D. Zhao and Y.-C. Cao, *Materials Today*, 2017, **20**, 258-266.

19. Y. Im, S. Y. Byun, J. H. Kim, D. R. Lee, C. S. Oh, K. S. Yook and J. Y. Lee, *Adv. Funct. Mater.*, 2017, **27**.

20. S. Jiao, Y. Liao, X. Xu, L. Wang, G. Yu, L. Wang, Z. Su, S. Ye and Y. Liu, *Adv. Funct. Mater.*, 2008, **18**, 2335-2347.

21. Best research-cell efficiencies, http://www.nrel.gov/pv/assests/images/efficiency-chart.png, accessed: July 2018

22. L. Meng, J. You, T. F. Guo and Y. Yang, *Acc. Chem. Res.*, 2016, **49**, 155-165.

View Article Online
DOI: 10.1039/C8TC01956H

Published on 27 July 2018. Downloaded by Kaohsiung Medical University on 7/27/2018 11:37:23 AM.

Journal of Materials Chemistry C Accepted Manuscript

23. T. Liu, K. Chen, Q. Hu, R. Zhu and Q. Gong, *Adv. Energy Mater.*, 2016, **6**, 1600457.

24. W. Yan, S. Ye, Y. Li, W. Sun, H. Rao, Z. Liu, Z. Bian and C. Huang, *Adv. Energy Mater.*, 2016, **6**, 1600474.

25. H. D. Pham, H. Hu, K. Feron, S. Manzhos, H. Wang, Y. M. Lam and P. Sonar, *Sol. RRL*, 2017, **1**, 1700105.

26. H. J. Snaith, A. Abate, J. M. Ball, G. E. Eperon, T. Leijtens, N. K. Noel, S. D. Stranks, J. T. Wang, K. Wojciechowski and W. Zhang, *J. Phys. Chem. Lett.*, 2014, **5**, 1511-1515.

27. X. Bao, Q. Zhu, M. Qiu, A. Yang, Y. Wang, D. Zhu, J. Wang and R. Yang, *J. Mater. Chem. A*, 2015, **3**, 19294-19298.

28. Z. Yu and L. Sun, *Adv. Energy Mater.*, 2015, **5**, 1500213-1500230.

29. F. Fu, T. Feurer, Thomas P. Weiss, S. Pisoni, E. Avancini, C. Andres, S. Buecheler and Ayodhya N. Tiwari, *Nat. Energy*, 2016, **2**, 16190.

30. Y.-K. Wang, Z.-C. Yuan, G.-Z. Shi, Y.-X. Li, Q. Li, F. Hui, B.-Q. Sun, Z.-Q. Jiang and L.-S. Liao, *Adv. Funct. Mater.*, 2016, **26**, 1375-1381.

31. N. H. Tiep, Z. Ku and H. J. Fan, *Adv. Energy Mater.*, 2016, **6**, 1501420.

32. Y. Shao, Y. Yuan and J. Huang, *Nat. Energy*, 2016, **1**, 15001.

33. J. H. Heo, H. J. Han, D. Kim, T. K. Ahn and S. H. Im, *Energy Environ. Sci.*, 2015, **8**, 1602-1608.

34. Y. Rong, L. Liu, A. Mei, X. Li and H. Han, *Adv. Energy Mater.*, 2015, **5**, 1501066.

35. K. W. Wong, H. L. Yip, Y. Luo, K. Y. Wong, W. M. Lau, K. H. Low, H. F. Chow, Z. Q. Gao, W. L. Yeung and C. C. Chang, *Appl. Phys. Lett.* , 2002, **80**, 2788-2790.

36. J. Wang, K. Liu, L. Ma and X. Zhan, *Chem. Rev.*, 2016, **116**, 14675-14725.

37. N. Marinova, S. Valero and J. L. Delgado, *J. Colloid Interface Sci.*, 2017, **488**, 373-389.

38. D. Bi, W. Tress, M. I. Dar, P. Gao, J. Luo, C. Renevier, K. Schenk, A. Abate, F. Giordano, J.-P. C. Baena, J.-D. Decoppet, S. M. Zakeeruddin, M. K. Nazeeruddin, M. Grätzel and A. Hagfeldt, *Sci. Adv.*, 2016, **2**, e1501170.

39. H. D. Pham, Z. Wu, L. K. Ono, S. Manzhos, K. Feron, N. Motta, Y. Qi and P. Sonar, *Adv. Electronic Mater.*, 2017, **3**, 1700139.

40. H. J. Snaith and M. Grätzel, *Appl. Phys. Lett.*, 2006, **89**, 262114.

41. J. Jang, S. Nam, K. Im, J. Hur, S. N. Cha, J. Kim, H. B. Son, H. Suh, M. A. Loth, J. E. Anthony, J.-J. Park, C. E. Park, J. M. Kim and K. Kim, *Adv. Funct. Mater.*, 2012, **22**, 1005-1014.

42. M. Chen, Y. Zhao, L. Yan, S. Yang, Y. Zhu, I. Murtaza, G. He, H. Meng and W. Huang, *Angew. Chem. Int. Ed. Engl.*, 2017, **56**, 722 –727.

43. J. Liu, J. Liu, Z. Zhang, C. Xu, Q. Li, K. Zhou, H. Dong, X. Zhang and W. Hu, *J. Mater. Chem. C*, 2017, **5**, 2519-2523.

44. H. Park, J. Lee, I. Kang, H. Y. Chu, J.-I. Lee, S.-K. Kwon and Y.-H. Kim, *J. Mater. Chem.*, 2012, **22**, 2695-2700.

45. C. Teng, X. Yang, C. Yang, S. Li, M. Cheng, A. Hagfeldt and L. Sun, *J. Phys. Chem. C*, 2000, **114**, 9101-9110.

View Article Online
DOI: 10.1039/C8TC01956H

Published on 27 July 2018. Downloaded by Kaohsiung Medical University on 7/27/2018 11:37:23 AM.

Journal of Materials Chemistry C Accepted Manuscript

46. J. Liu, H. Zhang, H. Dong, L. Meng, L. Jiang, L. Jiang, Y. Wang, J. Yu, Y. Sun, W. Hu and A. J. Heeger, *Nat. Commun.*, 2015, **6**, 10032.

47. X. Liu, F. Kong, R. Ghadari, S. Jin, T. Yu, W. Chen, G. Liu, Z. Tan, J. Chen and S. Dai, *Chem. Commun.*, 2017, **53**, 9558-9561.

48. S. Kazim, F. J. Ramos, P. Gao, M. K. Nazeeruddin, M. Grätzel and S. Ahmad, *Energy Environ. Sci.*, 2015, **8**, 1816-1823.

49. H. U. Kim, J. H. Kim, H. Kang, A. C. Grimsdale, B. J. Kim, S. C. Yoon and D. H. Hwang, *ACS Appl. Mater. Interfaces*, 2014, **6**, 20776-20785.

50. J. W. Jung, F. Liu, T. P. Russell and W. H. Jo, *Adv. Energy Mater.*, 2015, **5**.

51. C. Liu, W. Xu, X. Guan, H.-L. Yip, X. Gong, F. Huang and Y. Cao, *Macromolecules*, 2014, **47**, 8585-8593.

52. J. E. Anthony, *Angew. Chem. Int. Ed. Engl.*, 2008, **47**, 452-483.

53. P. Agarwala and D. Kabra, *J. Mater. Chem. A*, 2017, **5**, 1348-1373.

54. X. Zhao and M. Wang, *Materials Today Energy*, 2018, **7**, 208-220.

55. X. Yang, X. Xu and G. Zhou, *J. Mater. Chem. C*, 2015, **3**, 913-944.

56. T. T. Do, Y. E. Ha and J. H. Kim, *Org. Electron.*, 2013, **14**, 2673-2681.

57. S. Shinamura, I. Osaka, E. Miyazaki, A. Nakao, M. Yamagishi, J. Takeya and K. Takimiya, *J. Am. Chem. Soc.*, 2011, **133**, 5024-5035.

58. I. Osaka, S. Shinamura, T. Abe and K. Takimiya, *J. Mater. Chem. C*, 2013, **1**, 1297-1304.

59. T. Matsushima and C. Adachi, *Chem. Mater.*, 2008, 2881–2883.

60. S. C. Rasmussen, S. J. Evenson and C. B. McCausland, *Chem. Commun.*, 2015, **51**, 4528-4543.

61. F. Zhang, D. Wu, Y. Xu and X. Feng, *J. Mater. Chem.*, 2011, **21**, 17590–17600.

62. M. Saliba, S. Orlandi, T. Matsui, S. Aghazada, M. Cavazzini, J.-P. Correa-Baena, P. Gao, R. Scopelliti, E. Mosconi, K.-H. Dahmen, F. De Angelis, A. Abate, A. Hagfeldt, G. Pozzi, M. Graetzel and M. K. Nazeeruddin, *Nat. Energy*, 2016, **1**, 15017-15024.

63. Z. Ning and H. Tian, *Chem. Commun.*, 2009, DOI: 10.1039/b908802d, 5483-5495.

64. Y. Shirota, *J. Mater. Chem.*, 2005, **15**, 75-93.

65. Y. Shirota, *J. Mater. Chem.*, 2000, **10**, 1-25.

66. X. Liu, J. Liang, J. You, L. Ying, Y. Xiao, S. Wang and X. Li, *Dyes Pigm.*, 2016, **131**, 41-48.

67. P. Cias, C. Slugovc and G. Gescheidt, *J. Phys. Chem. A*, 2011, **115**, 14519-14525.

68. S. S. Reddy, V. G. Sree, H.-Y. Park, A. Maheshwaran, M. Song and S.-H. Jin, *Dyes Pigm.*, 2017, **145**, 63-71.

69. A. Cravino, P. Leriche, O. Alévêque, S. Roquet and J. Roncali, *Adv. Mater.*, 2006, **18**, 3033-3037.

70. Z. Zheng, Q. Dong, L. Gou, J.-H. Su and J. Huang, *J. Mater. Chem. C*, 2014, **2**, 9858-9865.

View Article Online
DOI: 10.1039/C8TC01956H

Published on 27 July 2018. Downloaded by Kaohsiung Medical University on 7/27/2018 11:37:23 AM.

Journal of Materials Chemistry C Accepted Manuscript

71. W. Liang, Z. Gao, W. Song, J. Su, K. Guo, Q. Dong, J. Huang and W.-Y. Wong, *Tetrahedron*, 2016, **72**, 1505-1510.

72. Y. Chen, W. Liang, W. H. Choi, J. Huang, Q. Dong, F. Zhu and J. Su, *Dyes Pigm.*, 2015, **123**, 196-203.

73. A. D. Becke, *J. Chem. Phys.*, 1993, **98**, 5648-5652.

74. P. Hohenberg and W. Kohn, *Phys. Rev.* , 1964, **136**, B864-B871.

75. W. Kohn and L. Sham, *Phys. Rev.* , 1965, **140**, A1133-A1138.

76. H. Usta, C. Kim, Z. Wang, S. Lu, H. Huang, A. Facchetti and T. J. Marks, *J. Mater. Chem.*, 2012, **22**, 4459-4472.

77. J. Wang, S. Wang, X. Li, L. Zhu, Q. Meng, Y. Xiao and D. Li, *Chem. Commun.*, 2014, **50**, 5829-5832.

78. X. Zhan, N. Sun, Z. Wu, J. Tu, L. Yuan, X. Tang, Y. Xie, Q. Peng, Y. Dong, Q. Li, D. Ma and Z. Li, *Chem. Mater.*, 2015, **27**, 1847-1854.

79. H. D. Pham, T. T. Do, J. Kim, C. Charbonneau, S. Manzhos, K. Feron, W. C. Tsoi, J. R. Durrant, S. M. Jain and P. Sonar, *Adv. Energy Mater.*, 2018, **8**, 1703007.

80. F. Zhang, C. Yi, P. Wei, X. Bi, J. Luo, G. Jacopin, S. Wang, X. Li, Y. Xiao, S. M. Zakeeruddin and M. Grätzel, *Adv. Energy Mater.*, 2016, **6**, 1600401.

81. R. Azmi, S. Y. Nam, S. Sinaga, Z. A. Akbar, C.-L. Lee, S. C. Yoon, I. H. Jung and S.-Y. Jang, *Nano Energy*, 2018, **44**, 191-198.

82. Y. D. Lin, B. Y. Ke, K. M. Lee, S. H. Chang, K. H. Wang, S. H. Huang, C. G. Wu, P. T. Chou, S. Jhulki, J. N. Moorthy, Y. J. Chang, K. L. Liau, H. C. Chung, C. Y. Liu, S. S. Sun and T. J. Chow, *ChemSusChem.*, 2016, **9**, 274-279.

83. R. Grisorio, R. Iacobellis, A. Listorti, L. De Marco, M. P. Cipolla, M. Manca, A. Rizzo, A. Abate, G. Gigli and G. P. Suranna, *ACS Appl. Mater. Interfaces*, 2017, **9**, 24778-24787.

84. A. Molina-Ontoria, I. Zimmermann, I. Garcia-Benito, P. Gratia, C. Roldan-Carmona, S. Aghazada, M. Graetzel, M. K. Nazeeruddin and N. Martin, *Angew. Chem. Int. Ed. Engl.*, 2016, **55**, 6270-6274.

85. A. Krishna, D. Sabba, H. Li, J. Yin, P. P. Boix, C. Soci, S. G. Mhaisalkar and A. C. Grimsdale, *Chem. Sci.*, 2014, **5**, 2702-2709.

86. X. Liu, F. Kong, T. Cheng, W. Chen, Z. Tan, T. Yu, F. Guo, J. Chen, J. Yao and S. Dai, *ChemSusChem.*, 2017, **10**, 968-975.

87. R. Grisorio, B. Roose, S. Colella, A. Listorti, G. P. Suranna and A. Abate, *ACS Energy Lett.*, 2017, **2**, 1029-1034.

88. J. Zhang, B. Xu, L. Yang, C. Ruan, L. Wang, P. Liu, W. Zhang, N. Vlachopoulos, L. Kloo, G. Boschloo, L. Sun, A. Hagfeldt and E. M. J. Johansson, *Adv. Energy Mater.*, 2018, **8**.

89. K. T. Cho, S. Paek, G. Grancini, C. Roldán-Carmona, P. Gao, Y. Lee and M. K. Nazeeruddin, *Energy Environ. Sci.*, 2017, **10**, 621-627.

90. J.-P. Correa-Baena, W. Tress, K. Domanski, E. H. Anaraki, S.-H. Turren-Cruz, B. Roose, P. P. Boix, M. Grätzel, M. Saliba, A. Abate and A. Hagfeldt, *Energy Environ. Sci.*, 2017, **10**, 1207-1212.

View Article Online
DOI: 10.1039/C8TC01956H

91. X. Li, M. Cai, Z. Zhou, K. Yun, F. Xie, Z. Lan, J. Hua and L. Han, *J. Mater. Chem. A*, 2017, **5**, 10480-10485.

92. J. Nelson, *The physics of solar cells.* 2003. Imperial College Press.

Published on 27 July 2018. Downloaded by Kaohsiung Medical University on 7/27/2018 11:37:23 AM.

Journal of Materials Chemistry C Accepted Manuscript

View Article Online
DOI: 10.1039/C8TC01956H

Published on 27 July 2018. Downloaded by Kaohsiung Medical University on 7/27/2018 11:37:23 AM.

TOC graph

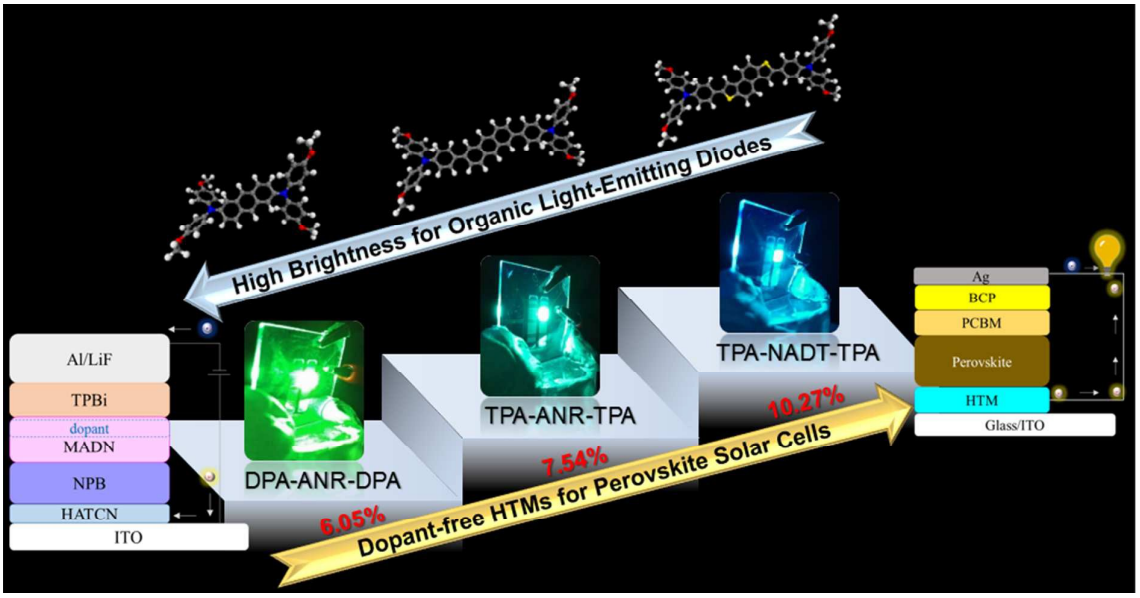

A series of strong electron-rich small molecules based acene were designed and synthesized for the purpose of green/blue organic light-emitting diodes and perovskite solar cells applications.

Journal of Materials Chemistry C Accepted Manuscript